



Provenance of aeolian sands from the southeastern Sahara from a detrital zircon perspective

Alexis Licht^{a,*}, Adrien Folch^{a,b}, Florence Sylvestre^{a,c}, Abdallah Nassour Yacoub^{a,c}, Nathan Cogné^d, Moussa Abderamane^c, Abel Guihou^a, Nario Mahamout Kisne^c, Jules Fleury^a, Pierre Rochette^a, Bertille Edith Bella Nké^e, Al-hadj Hamid Zagalo^f, Marc Poujol^d, Pierre Deschamps^a

^a Aix-Marseille Université, CNRS, IRD, INRAE, CEREGE, Aix-en-Provence, France

^b Freie Universität Berlin, Deutsche GeoForschungsZentrum (GFZ), Potsdam, Germany

^c Université de N'Djamena, Département de Géologie, Laboratoire Hydro-Géosciences et Réservoirs, N'Djamena, Chad

^d Université de Rennes, CNRS, Géosciences Rennes – UMR 6118, F-35000, Rennes, France

^e Laboratory of Geosciences and Sustainable Development, Faculty of Sciences University of Maroua, P.O. Box 814, Maroua, Cameroon

^f Université des Sciences et de Technologie d'Ati, Faculté des Sciences de la vie, de la Terre et de l'Aménagement du Territoire - Ati, Chad

ARTICLE INFO

Handling Editor: Dr Giovanni Zanchetta

Keywords:

Detrital zircon
Provenance
Desert
Source to sink
Sahara

ABSTRACT

Sahara sands have been proposed to result from the extensive and repetitive recycling of much older sedimentary rocks – a necessary mechanism to explain their petrographic maturity and the similarity of their detrital zircon populations at continental scale. Where and how this recycling occurs today remain poorly understood. This study investigates the source of modern sands from the southeastern Sahara by leveraging on a large ($n > 7800$) new dataset of detrital zircon ages from source rocks, modern and ancient dune fields in Chad and Cameroon. We show that zircon age populations show noticeable regional differences when analyzing a large n amount of ages, questioning the similarity of detrital zircon populations in Saharan sands. Dune fields from the driest parts of our sampling area have distinct age distributions that imply discrete sources with differences in bedrock zircon age populations at regional (several 100 km) scale. In the wetter, Sahelian part of our sampling area, the zircon age distribution of dune fields is best-explained by a significant contribution of recent alluvium from local wadis and rivers to the aeolian sedimentary budget. The origin of aeolian sands in the southeastern Sahara is thus local and polygenetic. Recycling of older sedimentary rocks via physical abrasion is only prominent in the driest parts of our sampling area and does not result in the homogenization of Saharan sands.

1. Introduction

Two mechanisms are commonly proposed for the generation of vast sand seas: the deflation of "fresh" fluvial alluvium in arid floodplains and deltas (Stevens et al., 2013; Garzanti et al., 2014), and the physical abrasion and recycling of older sandstones, a mechanism that is necessary to generate pure quartzose sand (Garzanti et al., 2013; King, 2019). Identifying the relative contribution of both processes and the locations where they are most active are essential to understanding the morphology, petrology, and overall dynamics of modern and ancient deserts (Courrech du Pont et al., 2014; Bertolini et al., 2023). These research questions are frequently addressed with sedimentary provenance tools such as sand petrographic analysis, bulk or single-grain

geochemical fingerprinting (Stevens et al., 2013; Garzanti et al., 2013, 2014; Rittner et al., 2016; Pastore et al., 2021). Tracking the areas of eolian sand generation in modern and ancient dune fields can be challenging when using these approaches. Indeed, the reworking of fluvial material by winds can result in mistaking fluvial transport for aeolian transport and confuses the actual source of the aeolian material (Licht et al., 2016a). Furthermore, regular recycling of older sandstones results in a regional homogenization of sandstone petrography and geochemistry, sometimes at continental scale, making it impossible to precisely determine the source of the sands (Garzanti et al., 2013; Pastore et al., 2021). This latter process is evoked to explain the extraordinary similarity of Sahara Desert sands, especially in its southern part where they display similar petrographic grain counts, heavy mineral assemblages,

* Corresponding author.

E-mail address: licht@cerege.fr (A. Licht).

<https://doi.org/10.1016/j.quascirev.2024.108539>

Received 8 November 2023; Received in revised form 15 January 2024; Accepted 4 February 2024

Available online 16 February 2024

0277-3791/© 2024 The Authors. Published by Elsevier Ltd. This is an open access article under the CC BY-NC license (<http://creativecommons.org/licenses/by-nc/4.0/>).

and zircon U–Pb age populations; [Pastore et al. \(2021\)](#) interpret this continental-scale homogenization as resulting from a long-term abrasion and recycling of the continent-wide blanket of Cambro-Ordovician sandstones from Mauritania to Arabia.

Although this interpretation is sound at continental scale, its validity for southeastern Saharan ergs, including the wide dune fields covering the Lake Chad Basin such as the Djourab and Kanem dune fields, as well as in the numerous paleo-dune fields further south found up to Cameroon, is questionable ([Fig. 1a](#)). Indeed, Cambro-Ordovician rocks barely crop out in the wide yardang (linear eolian erosional feature) fields of the Erdi Plateau, on the pathways of the upstream trade winds (Harmattan winds), and are thus poor candidates for the regional sources of these sands ([Fig. 1b](#)). Moreover, numerous wadis (dry creeks) and perennial rivers drain central and southern Chad, carrying alluvium at the edge of modern and ancient ergs. The area has regularly experienced wetter episodes during the Quaternary, including recently (early to middle Holocene), and was occupied by the wide Lake Mega-Chad and its associated river drainages (e.g. [Ghienne et al., 2002](#); [Schuster et al., 2005](#); [Bouchette et al., 2010](#); [Armitage et al., 2015](#)). The contribution of a potential fluvial sediment input from these river systems has not been investigated. The source of southeastern Saharan sand is yet critical to understand because the Bodélé Depression, straddling Chadian dune fields, is the largest single area of dust production in the world, enhanced by the abrasion generated by sand-loaded winds ([Washington et al., 2006](#)).

The southeastern Sahara encompasses a single African craton, the Saharan Metacraton ([Kusnir, 1995](#)), which was fully assembled before Panafrican (late Neoproterozoic) times ([Isseini et al., 2012](#)). In cratonic areas, detrital zircon grains often show the same U–Pb age populations on a regional scale, making hopeless the search for fingerprinting-populations that could be used for provenance tracking ([Licht et al., 2016a](#)). However, each age population can be locally expressed in varying proportions. These variations depend on the local tectono-magmatic history (ie: varying intensity of magmatic episodes)

and on the subsequent history of sediment mixing and recycling (ie: long-distance drainages providing sediment from distant areas, that is later incorporated into local sediment through recycling). Tracking regional variations in the proportion of zircon age populations and using it to track changes in provenance yet require a significant amount of zircon ages per sample/per area ($n > 500$ – 800 , depending on the amount of individual age populations; [Pullen et al., 2014](#)).

This study utilizes the statistical advantages of "large n " single mineral geochronology to address the provenance of aeolian zircon grains from the southeastern Sahara. We provide new zircon U–Pb ages from modern and ancient aeolian dunes from Chad and northern Cameroon, as well as from bedrocks and river sediment to characterize their source areas. We then investigate through mixture modeling if increasing the regional zircon age dataset allows us to better identify aeolian sediment sources.

2. Samples and methods

We focused our sampling around an approximate NE-SW transect following the direction of Harmattan winds, from the desertic Erdi Plateau (mean annual precipitation < 50 mm) to the Sahelian parts of Chad and northern Cameroon (annual precipitation > 200 mm; [Fig. 1a](#)). All samples are located in today's Lake Chad drainage basin, with some falling within the maximum extent of the last Lake Mega-Chad episode (early to mid-Holocene; [Armitage et al., 2015](#)). Two to three kg of sand were collected on modern aeolian dunes, including, from north to south: five samples at the southern edge of the Erdi Plateau; seven samples in the Djourab Desert; four samples in the Bahr el Ghazal area, south of the Djourab Desert; and six samples in the Kanem Desert. Samples from ancient, inactive dunes were also analyzed, including: two samples from buried aeolian sandstones exposed at the base of a cliff which is dated to 4.2 ± 0.2 Myr by authigenic ^{10}Be dating (Kouba Olanga section, [Leblatard et al., 2010](#)); three samples from vegetalized sand-ridges associated with the last Lake Mega-Chad episode, dominantly made of aeolian

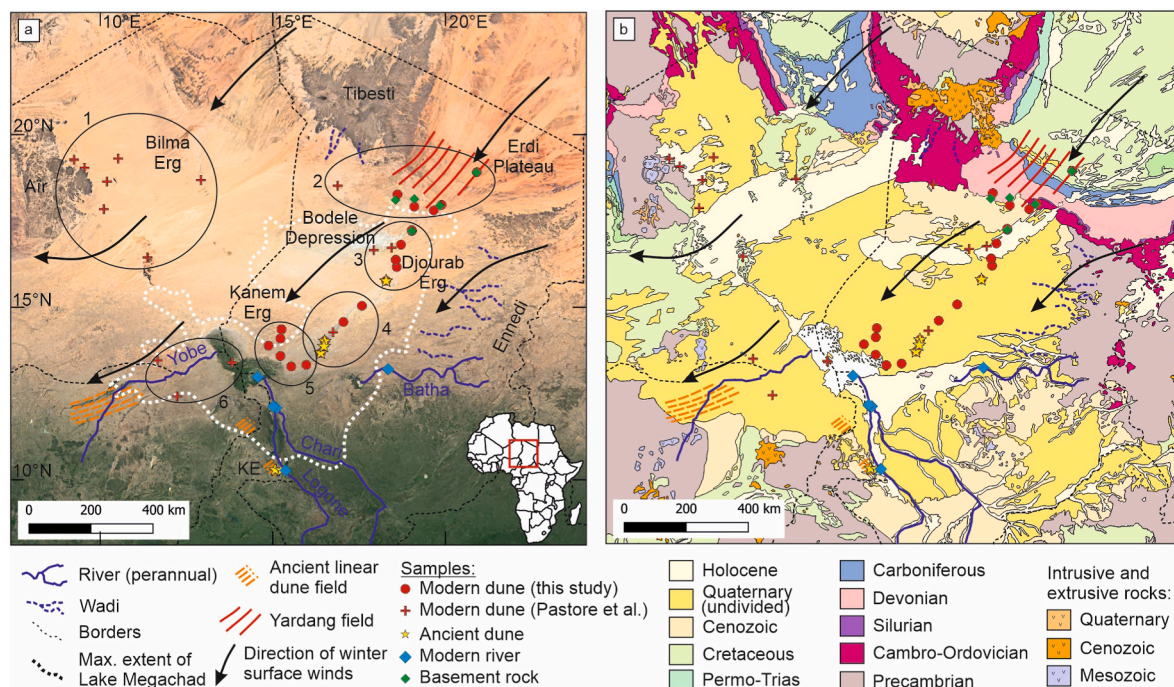


Fig. 1. (a) Main geomorphological features of the southeastern Sahara, with sampling locations for basement rocks, modern river sediment (including one sample from [Shellnutt et al., 2019](#)), ancient and modern dunes (from this study and from [Pastore et al., 2021](#)). The location of the figure on the African continent is highlighted by a red square on the African map in the bottom right corner. Winter wind directions from [Engelstaedter and Washington \(2007\)](#). Max extent of Chad Paleolake from [Ghienne et al., \(2002\)](#). KE: Kalfou Erg. Circles correspond to sample grouping on [Fig. 2](#): 1: Bilma Desert; 2: Southern Erdi Plateau; 3: Djourab Desert; 4: Bahr el Ghazal area; 5: Southern Kanem Desert; 6: southern Lake Chad. (b) geological map of the same area ([Persits et al., 1997](#)).

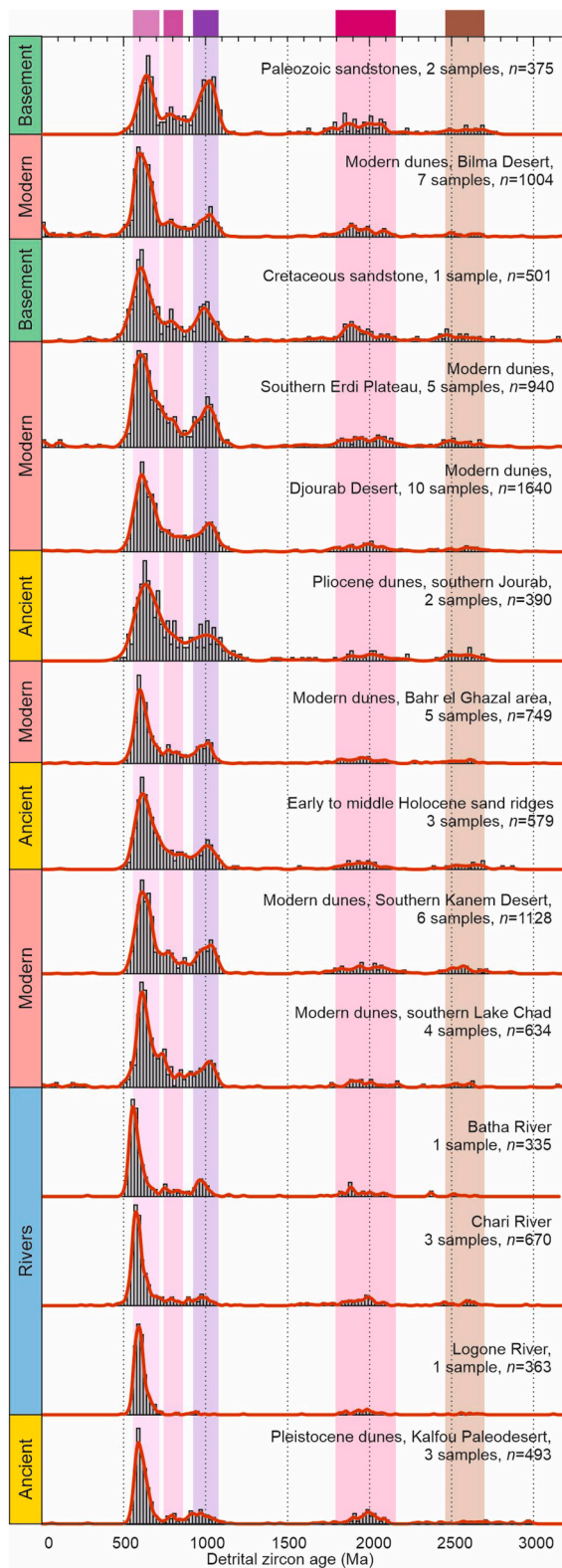


Fig. 2. Compiled age distribution (histograms; bins of 20 Myr) and kernel density estimates (red lines) of basement rocks (in green), modern (in pink) and ancient (in yellow) aeolian sediment, and river sediment (in blue) from Southeastern Sahara, arranged from north (top) to south (bottom); names of samples included in each compilation on Fig. S1). Purple to brown shades highlight the five main age populations identified here: late Panafrican (560–720 Ma), early Panafrican population (740–860 Ma), Grenvillian (920–1080 Ma), Eburnean (1800–2160 Ma), and Liberian (2460–2700 Ma).

sands with occasional evidence for reworking in a coastal environment (Ghienne et al., 2002); and three samples from vegetalized linear dunes of the Kalfou Erg in northern Cameroon, an ancient desert attributed to the last glacial maximum (Seignobos and Iyébi-Mandjek, 2017). At the northern edge of our sampling transect (the southern edge of the Erdi Plateau), where numerous yardangs have been carved by Harmattan winds, we sampled basement sandstones including one Cambrian sample, one Devonian sample, one Cretaceous sample (Nubian sandstone), one Cenozoic sample (Continental Terminal formation), and one Quaternary sandstone (desert pavement; see Fig. 1b and Kusnir, 1995, for stratigraphic details). Further south, we sampled modern river sediments to represent the signature of regional alluvium: one sample from the Batha River, one from the Logone River, one from the Chari River ca. 100 km from its mouth and one in the delta itself.

These samples were separated by standard heavy liquid techniques and mounted in epoxy resin; laser spots were selected randomly ("blind-dating" approach, e.g. Pastore et al., 2021); selected zircon grains were then dated by laser ablation inductively coupled plasma mass spectrometry (LA-ICP-MS) at the Envitop analytical facility at CEREGE (Centre for Research and Education in Environmental Geosciences), with an Element XR ICP-MS connected to an ESI laser (ArF 193 nm) ablation system. Zircons were ablated with a 25 μm spot diameter, 15 Hz pulse repetition rate, an energy fluence of 1.5 J/cm² and a carrier gas flow of 0.975 L/min, using zircon 91500 as primary reference material (Wiedenbeck et al., 1995). Data reduction, dates and date uncertainties calculation were conducted with an in-house MATLAB script; details about our U–Pb dating workflow and data reduction steps are given in Supplementary File 1. Our data reduction workflow combines steps from previously published procedures, including the calculation of excess variance (Paton et al., 2010), the consideration of signals coming from different detectors (Pullen et al., 2018), and the impact of ²⁰⁷Pb beam intensity on date uncertainties (Matthews and Guest, 2017). The three zircon validation reference materials used during these sessions yielded offset around TIMS ages <1% in most cases, <2% otherwise. Four samples were also analyzed via LA-ICP-MS at the GeOHeLiS platform (University of Rennes, France); details about the analytical set-up and U–Pb dating workflow at GeOHeLiS are given in Supplementary File 2. Briefly, data were acquired using a quadrupole Agilent 7700 \times ICP-MS coupled to an ESI NWR193UC Excimer laser, employing a 25 μm laser spot with a repetition rate of 4 Hz and energy of 5 J/cm² for a duration of 45 s. Zircon 91500 (Wiedenbeck et al., 1995) was also used as primary reference material, and GJ-1 (Jackson et al., 2004) as quality control reference material. Data were reduced using Iolite v4.5 (Paton et al., 2011). GJ-1 yielded concordant data in accordance with the reference age for all individual sessions and a global concordant age of 601.3 \pm 1.1 Ma ($n = 70$, MSWD = 0.65).

The discordance filter used to screen for concordant grains is the Concordia distance of Vermeesch (2021) using isometric logratios and a threshold of 10 (SI) for discordance and 5 (SI) for reverse discordance. Ages used for plotting are the Concordia age of Vermeesch (2021). Age uncertainties are given with and without the systematic uncertainty calculated over multiple sessions (1.3 % 2s at CEREGE and 1.6 % 2s at GeOHeLiS for ²³⁸U/²⁰⁶Pb ratios). In total, our dataset includes 9969 ages from 36 samples, including 7886 concordant ages. Detailed data are available in Supplementary Table 1.

3. Results

Individual age distributions are displayed in Supplementary Fig. S1, together with data from the Chari River sample from Shellnutt et al. (2019), and other data from the region previously published by Pastore et al. (2021). These other data include modern dunes from the Djourab Desert and Bahr El Ghazal areas, dunes from the southern shore of modern Lake Chad and further south in Nigeria, and dunes from the Bilma Desert in Niger (see Fig. 1). Note that we used the same zircon ages (Concordia age) and applied the same discordance filter to all

external data. Compiled age distributions are displayed on Fig. 2.

Regardless of their location, all samples and sample compilations display the same four age populations corresponding to global orogenic episodes: late Panafrican (560–720 Ma), Grenvillian (920–1080 Ma), Eburnean (1800–2160 Ma), and Liberian (2460–2700 Ma). A distinct early Panafrican population (740–860 Ma) is also sometimes observable, although its contribution is marginal compared to the later Panafrican population (560–720 Ma). Phanerozoic grains are barely present in the samples; Meso-Cenozoic grains are only present in notable proportions (4%) in samples of the Bilma Desert, more minorly in the southern part of the Erdi Plateau and south of Lake Chad (Figs. 3 and 4)

The late Panafrican and Grenvillian age populations are present in quasi-similar proportion in the Paleozoic sandstones; the contribution of Grenvillian ages significantly decreases in younger sandstones, while the contribution of late Panafrican ages increases (Fig. S1). This trend is also geographically observable in the compiled age distributions (Fig. 3), with a well-marked gradual increase in the proportion of late Panafrican vs Grenvillian ages (Fig. 3) from north to south. The lowest contribution of Grenvillian ages and highest contribution of late Panafrican ages are found in modern river sediments in southern Chad, where the Grenvillian population is poorly expressed; it is quasi-absent in Logone River sediment (Fig. 2).

Two outliers to this trend are noticeable (Fig. 3): samples from the

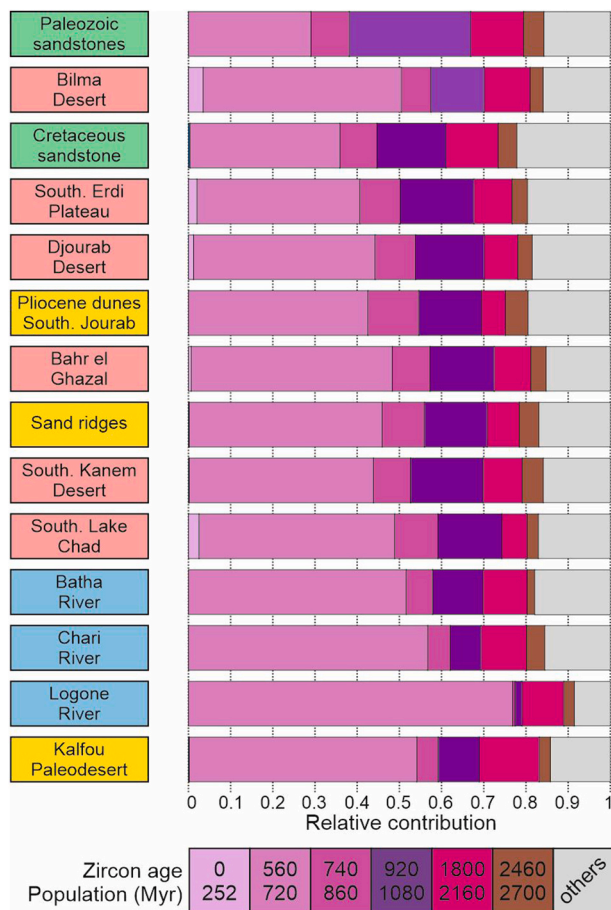


Fig. 3. Relative contribution of Meso-Cenozoic (0–252 Ma), late Panafrican (560–720 Ma), early Panafrican population (740–860 Ma), Grenvillian (920–1080 Ma), Eburnean (1800–2160 Ma), and Liberian (2460–2700 Ma) ages to the compiled age distributions of Fig. 2, highlighted with purple to brown colors (same coding as on Fig. 2); the grey color corresponds to zircons that do not belong to the six age populations. Samples are arranged from north (top) to south (bottom) and are separated like on Fig. 2 in basement rocks (in green), modern (in pink) and ancient (in yellow) aeolian sediment, and river sediment (in blue).

Bilma Desert display a high proportion of late Panafrican ages compared to the samples from northern Chad; Bilma Desert samples are yet located further west, outside the Harmattan wind pathway coming from the Erdi Plateau (Fig. 1a). Samples from the Kalfou Desert display a lower contribution of late Panafrican ages compared to the nearby sample from the Logone River (Fig. 1a); their age distribution and age population proportions resemble the ones of the Chari River (Figs. 2 and 3).

When plotted on a multidimensional scaling (MDS) plot, individual samples broadly plot on a line with Paleozoic sandstone samples on one end and River sediment samples on the other end (Fig. 4). Samples from northern Chad plot near the Paleozoic sample field, while samples from southern Chad and Cameroon plot near the river sediment one. Samples plotting outside this line are characterized by a higher number of Meso-Cenozoic grains (Fig. S1), including the majority of the Bilma Desert samples.

4. Discussion

4.1. Mixture modeling of Saharan Metacraton sands

All samples studied here (dunes, river sediment, bedrock) display the same age populations and only differ in the relative proportion between Panafrican vs Grenvillian ages. The high proportion of Grenvillian ages in the northern part of our sampling area, and particularly well expressed in the Paleozoic rocks, has already been noticed by Meinhold et al. (2011) for southern Libya; their presence in the Paleozoic rocks has been explained by long-distance sediment transport from neighboring cratons, possibly by glacial processes (Le Heron, 2018). This long-distance transport would have ceased during the Mesozoic, explaining the observed decrease of Grenvillian populations in younger sedimentary rocks. By contrast, the prominence of Panafrican ages in the southern parts of the Saharan Metacraton, as witnessed in the river sediments of southern Chad, has been explained by a late Panafrican magmatic flare-up that would have only affected the southern edge of the metacraton (Shellnutt et al., 2019). The upstream drainage basin (Mayo Kebi region) of the Logone River is indeed mostly made of Panafrican magmatic rocks (Penaye et al., 2006).

The large n age amount for most of the areas and types of sediment (n from 300 to 1600) allow us to highlight that the regional changes found in Saharan Metacraton basement rocks are also found in modern and ancient dunes. The proportion of Panafrican vs Grenvillian ages gradually increases towards the south, a trend already noticed by Pastore et al. (2021) in dunes at a continental scale. This proportion always lies between two extreme geographic poles represented by the Paleozoic sandstones in the north (high content in Grenvillian ages) and the Logone River in the south (almost no Grenvillian age).

To test the idea that the age distribution of most aeolian samples can be explained by a simple mixture between these two extreme poles, we develop a mixture algorithm following the protocol proposed by Licht et al. (2016a,b). For each possible combination of the two poles (for instance, Paleozoic sandstones: 56%, Logone River: 44%), we modeled N synthetic age distributions of 150 ages (the average age amount per sample in modern zircon datasets) by randomly picking the necessary amount of ages in the age population of the two poles. N was chosen to be large enough to reproduce the potential variability in age proportions created by zircon subsampling ($N = 200$; Licht et al., 2016a). We then calculated the average statistical dissimilarity between each of these N synthetic age distributions and the age distribution of individual samples, as well as the regionally compiled age distributions. We used two different dissimilarity measures: the coefficient of non-determination, which is the complement of the cross-correlation coefficient of probability density plots ($1-R^2$) and has been shown to be the most efficient dissimilarity indicator for databases with varying n (Saylor and Sundell, 2016), and the Kolmogorov-Smirnov statistic, a classical dissimilarity indicator regularly used in detrital zircon studies (Vermeesch, 2013; Licht et al., 2016a; Pastore et al., 2021).

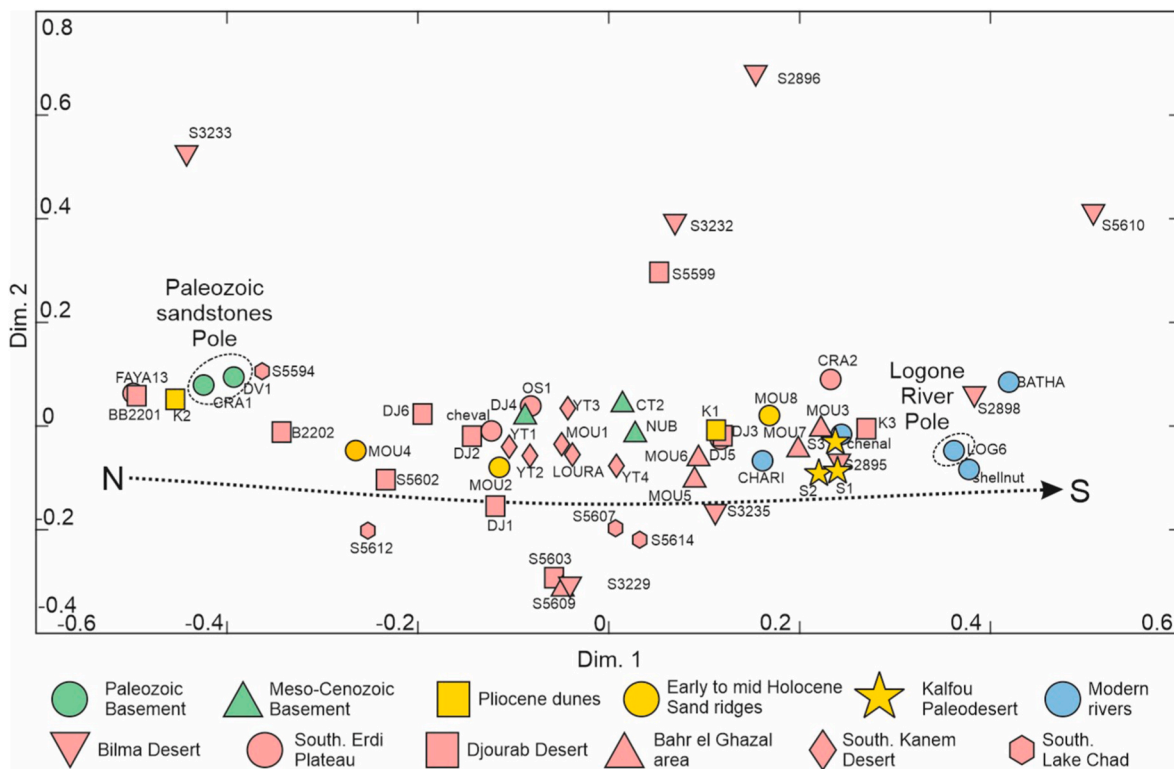


Fig. 4. Two-dimensional multidimensional scaling (MDS) plot of the analyzed samples from the southeastern Sahara (individual age distribution on [Supplementary Fig. S1](#)). Dissimilarity was calculated as the complement of the Cross-correlation coefficient of probability density plots ($1-R^2$), following [Saylor and Sundell \(2016\)](#) and [Saylor et al. \(2018\)](#). Stress of the MDS plot = 0.127. Shepard plot of the MDS on [Supplementary Fig. S2](#). The two provenance poles of [Fig. 5](#) are highlighted with dashed circles, as well as the overall N-S distribution of the samples (dashed line).

For most individual samples ([Fig. S3](#)) and all zircon age compilations ([Fig. 5](#)) of modern or ancient deserts, we can find a specific combination of the two poles that brings both dissimilarity measures below 0.1, indicating a close fit. These specific combinations are most of the time similar for both dissimilarity measures. For these combinations, a significant proportion (>50%, and commonly >75%) of the N randomly generated mixtures are statistically identical to the age distribution of the tested sample or age compilation sensu the K-S statistic at 95% confidence. For the Southern Erdi Plateau, Djourab Desert, southern Kanem Desert, the Pliocene dunes of the southern Djourab Desert, and the Holocene sand ridges of the Bahr el Ghazal area, prominent (>50%) statistical similarity is reached for a contribution between 60 and 80 % of Paleozoic sandstones zircon grains ([Fig. 5](#)); this proportion is similar to what is found for our Cretaceous (Nubian) sandstone sample. For the Bilma Desert, Bahr el Ghazal dunes, and dunes south of the Lake Chad, this contribution is lower, between 40 and 60%. The contribution of Paleozoic sandstones for Quaternary dunes from the Kalfou Paleodesert goes down to 30–60% and gets close to the contribution best explaining the age distribution of the Chari River, with only 20–50 %. We thus argue that the southeastern Sahara aeolian sediment is not homogenized by the continuous recycling of basement rocks, and that differences do persist at a sub-regional scale (100 km scale). These differences are yet difficult to identify due to the overall consistency of zircon age populations found on the Sahara Metacraton, and can only be evidenced at high n zircon amount, as done in this study.

4.2. Implications for the provenance of southeastern Saharan desert sands

The age compilations from northern and central Chad deserts (Southern Erdi Plateau, Djourab Desert, southern Kanem Desert) are best explained by a combination of the two provenance poles that is similar to the one of the Nubian sandstone sample of the Erdi Plateau.

The Nubian sandstone is the dominant rock currently carved by yardangs on the Erdi Plateau ([Fig. 1a](#)) and is thus a good candidate for the source of the desert sands. An aeolian contribution from sands flown from southern Libya, from the Kufra Basin north of the Erdi Plateau, cannot be completely excluded in the absence of comparison samples from southern Libya; we note however that the Nubian sandstone is also the dominant exposed rock in the Kufra Basin. We thus argue that physical abrasion of the Nubian Sandstone is likely the main process for sand generation for the northern and central Chad deserts, in and around the Bodélé Depression. The same can be proposed for the Pliocene dunes of the southern Djourab Desert, and the Holocene sand ridges of the Bahr el Ghazal area.

Further south, the Bahr el Ghazal aeolian sands, the dunes south of the Lake Chad and in the Kalfou Paleodesert display a higher contribution of Panafrican ages suggesting a contribution from local basement rocks (Panafrican granites and earlier metamorphic rocks) or alluvium from nearby river and wadi systems. We note, after a basic survey on satellite maps via GoogleEarth, that yardangs significantly shrink and disappear south of the Erdi Plateau, in the Ennedi foothills ([Fig. 1a](#)). By contrast, modern and ancient wadis are numerous in this region ([Schuster et al., 2005](#)). We thus suggest that the provenance of these dunes reflects some degree of mixing with alluvium deflated from Ennedi wadis and/or from the floodplains of the perennial rivers found further south. The contribution of alluvium is likely the greatest for sands from the Kalfou Paleodesert, which display an age distribution very similar to the one of the Chari River and is found directly next to the southwest of the Logone and Chari floodplains, downstream easterly winds.

Finally, Bilma Desert sands display a contribution of Panafrican ages that is higher than other dune fields at their latitude, as well as a noticeable population of Meso-Cenozoic grains; their dissimilarity with any other sample investigated in this study is well illustrated on the MDS

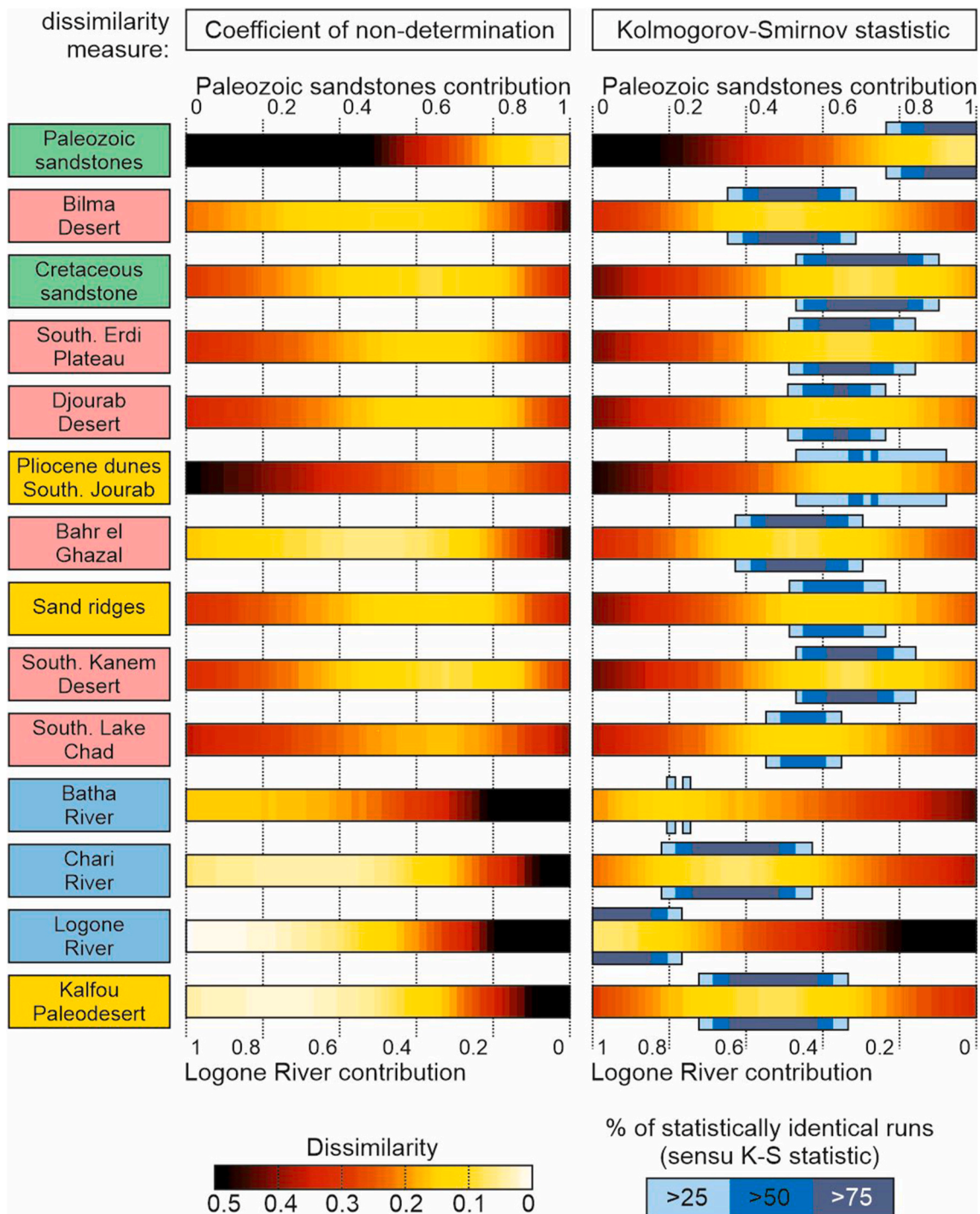


Fig. 5. Average dissimilarity between regionally compiled age distributions and randomly generated mixtures of zircon ages from Paleozoic sandstones and Logone River sediments. The first dissimilarity measure is the coefficient of non-determination (see main text) and is a dimensionless quantity between 0 and 1, with 0 indicating a perfect fit and 1 a complete misfit (Saylor and Sundell, 2016). The second dissimilarity measure is the Kolmogorov-Smirnov statistic (Vermeesch, 2013), which is a dimensionless, positive quantity with 0 indicating a perfect fit and getting higher with increasing misfit (Saylor and Sundell, 2016). We also display in blue shades the percentage (>25, >50, and >75%) of randomly generated mixtures that are statistically identical to each compiled age distribution (statistical similarity sensu the Kolmogorov-Smirnov statistic at the 95% confidence level; Licht et al., 2016a).

plot (Fig. 4). This misfit likely indicates a different source than the ones of the Chadian dune fields, that is likely to be found west and north of the Tibesti Mountains, where Cambro-Ordovician and Cenozoic magmatic rocks are more exposed (Deniel et al., 2015), upstream the easterly winds in Niger (Fig. 1a). Alternatively, this higher contribution of Panafrican ages could reflect the erosion of the local basement in Niger, including from the nearby Air Mountains, where Panafrican

magmatic rocks are prominent (Liégeois et al., 1994), and Cenozoic magmatic rocks present (Fig. 1).

Transport-induced grain-size fractionation in sediment has been shown to impact detrital zircon age distributions, especially in river sediment (Lawrence et al., 2011). Grain-size fractionation could occur in aeolian sands, as coarser sands transported via creep processes travel less than finer sands transported by saltation (Lancaster, 1986). The

regional differences observed here in zircon age distributions could be alternatively interpreted in terms of regional changes in prominent sand transport mode and associated changes in sand grain-size. Such regional grain-size changes remain to be documented in the southeastern Sahara. We did not visually notice any significant grain-size variation in our sample set. Our sampling focused on dune crests and upper lee faces, and we avoided sampling interdune spaces where coarser sands accumulate. We thus argue that grain-size fractionation effects are likely negligible in our U–Pb dataset, though this remains to be confirmed with a thorough granulometry study.

5. Conclusions

Our dataset allows us to show that the homogenization of Saharan zircon age populations at continental scale, emphasized by Pastore et al. (2021), is an artifact that can be lifted using a large n analysis. We demonstrated that the contribution of these age populations varies at the scale of several hundreds of kilometers and that these variations are also found in Sahara aeolian sands.

Our statistical analysis tracks back the origin of northern Chad desert sands to the recycling of the Nubian sandstones at the edge of the Erdi Plateau, and confirms the prevalence of physical abrasion as the prominent sand generator in the driest parts of the Sahara. Nonetheless, we show that the deserts of northern Chad and dune fields from the nearby Bilma Desert display different proportions of Panafrican and Meso-Cenozoic zircon grains, likely indicating different sources east and west of the Tibesti Mountains. Extensive recycling of regional sands after the end of the Neoproterozoic, a mechanism proposed to explain the petrographic maturity of Saharan sands (Pastore et al., 2021), is thus not advanced enough to erase regional differences in zircon age distributions.

Our dataset also highlights a gradual southward increase of Panafrican zircon grains in aeolian dunes which is best explained by an increased contribution of local alluvium to the provenance of the sands. This southward increase of alluvium input makes sense as aeolian dunes reach the wetter areas of the Sahel, where ancient and modern wadis are more numerous. Such an increase has also been observed along the rim of the Arabian Desert (Garzanti et al., 2017). The contribution of Chadian wadis to the sedimentary budget of Saharan sands remains to be confirmed by a detailed sand petrographic and grain-size study, which is beyond the scope of this paper. A multi-technique approach, including the study of other, less resistant heavy minerals, could better characterize the contribution of fresh alluvial material to the aeolian budget. Nonetheless, our work highlights previously unnoticed regional provenance variations, and emphasizes that large n zircon datasets can bring to light differences in sedimentary provenance that are invisible when using the common zircon amount found in classical detrital zircon studies ($n = \text{ca. } 150$ per sample).

Authors contribution

All authors have made substantial contributions to the study and approved the submitted manuscript.

AL designed the study, sampled and acquired the U–Pb data and wrote the manuscript.

FS, AY, MA, NM, PR, BN and AZ contributed to the sampling.

AF, NC, and AG contributed to the data acquisition.

NC, AG, MP and PD contributed to the data validation and interpretation.

Declaration of competing interest

The authors declare that they have no known competing financial interests or personal relationships that could have appeared to influence the work reported in this paper.

Data availability

All data are available in the supplementary material.

Acknowledgments

CEREGE Envitop analytical facility has received funding from “Excellence Initiative” of Aix Marseille University A*MIDEX - DATCARB project, a french “Investissement d’avenir” program. We thank the Centre National pour le Recherche et le Développement au Tchad, the French Embassy in Chad, and the IRD for their logistical support. We also thank I. Abakar Youssouf, J. Dauvier, J. Longerey and F. Demory for their assistance in the lab; Ahounta Dave, Mahamat Adoum, Haroun Soumaine, Silas, and Yves Gauthier for their assistance in the field.

Appendix A. Supplementary data

Supplementary data to this article can be found online at <https://doi.org/10.1016/j.quascirev.2024.108539>.

References

- Armitage, S.J., Bristow, C.S., Drake, N.A., 2015. West African monsoon dynamics inferred from abrupt fluctuations of Lake Mega-Chad. *Proc. Natl. Acad. Sci. USA* 112 (28), 8543–8548.
- Bertolini, G., Hartley, A.J., Marques, J.C., Paim, J.C., 2023. Controls on grain-size distribution in an ancient sand sea. *Sedimentology* 70 (4), 1281–1301.
- Bouchette, F., Schuster, M., Ghienne, J.-F., Denamiel, C., Roquin, C., Moussa, A., Marsaleix, P., Düringer, P., 2010. Hydrodynamics in Holocene Lake Mega-Chad. *Quat. Res.* 73 (2), 226–236.
- Courrech du Pont, S., Narteau, C., Gao, X., 2014. Two modes for dune orientation. *Geology* 42 (9), 743–746.
- Deniel, C., Vincent, P.M., Beauvilain, A., Gourgaud, A., 2015. The Cenozoic volcanic province of Tibesti (Sahara of Chad): major units, chronology, and structural features. *Bull. Volcanol.* 77 (9), 74.
- Engelstaedter, S., Washington, R., 2007. Atmospheric controls on the annual cycle of North African dust. *J. Geophys. Res. Atmos.* 112 (D3).
- Ghienne, J.F., Schuster, M., Bernard, A., Düringer, P., Brunet, M., 2002. The Holocene giant Lake Chad revealed by digital elevation models. *Quat. Int.* 87 (1), 81–85.
- Garzanti, E., Vermeesch, P., Andò, S., Vezzoli, G., Valagussa, M., Allen, K., et al., 2013. Provenance and recycling of Arabian desert sand. *Earth Sci. Rev.* 120, 1–19.
- Garzanti, E., Vermeesch, P., Andò, S., Lustrino, M., Padoan, M., Vezzoli, G., 2014. Ultra-long distance littoral transport of Orange sand and provenance of the Skeleton Coast Erg (Namibia). *Mar. Geol.* 357, 25–36.
- Garzanti, E., Vermeesch, P., Al-Ramadan, K.A., Andò, S., Limonta, M., Rittner, M., Vezzoli, G., 2017. Tracing transcontinental sand transport: from anatolia-zagros to the Rub’Al khali sand sea. *J. Sediment. Res.* 87 (11), 1196–1213.
- Isseni, M., André-Mayer, A.-S., Vanderhaeghe, O., Barbey, P., Deloule, E., 2012. A-type granites from the Pan-African orogenic belt in south-western Chad constrained using geochemistry, Sr–Nd isotopes and U–Pb geochronology. *Lithos* 153, 39–52.
- Jackson, S.E., Pearson, N.J., Griffin, W.L., Belousova, E.A., 2004. The application of laser ablation-inductively coupled plasma-mass spectrometry to in situ U–Pb zircon geochronology. *Chem. Geol.* 211 (1–2), 47–69.
- King, J., 2019. chapter 3: Wind Erosion. In: Livingstone, I., Warren, A. (Eds.), *Aeolian geomorphology: a new introduction*, pp. 61–79.
- Kusnir, I., 1995. Géologie, ressources minérales et ressources en eau du Tchad, second ed. Centre national d’appui à la recherche.
- Lancaster, N., 1986. Grain-size characteristics of linear dunes in the southwestern Kalahari. *J. Sediment. Res.* 56 (3), 395–400.
- Lawrence, R.L., Cox, R., Mapes, R.W., Coleman, D.S., 2011. Hydrodynamic fractionation of zircon age populations. *GSA Bulletin* 123 (1–2), 295–305.
- Lebatard, A.E., Bourlès, D.L., Braucher, R., Arnold, M., Düringer, P., Jolivet, M., et al., 2010. Application of the authigenic $^{10}\text{Be}/^{9}\text{Be}$ dating method to continental sediments: reconstruction of the Mio-Pleistocene sedimentary sequence in the early hominid fossiliferous areas of the northern Chad Basin. *Earth Planet. Sci. Lett.* 297 (1–2), 57–70.
- Le Heron, D.P., 2018. An exhumed Paleozoic glacial landscape in Chad. *Geology* 46 (1), 91–94.
- Licht, A., Pullen, A., Kapp, P., Abell, J., Giesler, N., 2016a. Eolian cannibalism: reworked loess and fluvial sediment as the main sources of the Chinese Loess Plateau. *GSA Bulletin* 128 (5–6), 944–956.
- Licht, A., Dupont-Nivet, G., Pullen, A., Kapp, P., Abels, H.A., Lai, Z., et al., 2016b. Resilience of the Asian atmospheric circulation shown by Paleogene dust provenance. *Nat. Commun.* 7 (1), 12390.
- Liégeois, J.P., Black, R., Navez, J., Latouche, L., 1994. Early and late Pan-African orogenies in the Air assembly of terranes (Tuareg shield, Niger). *Precambrian Res.* 67 (1–2), 59–88.

- Mathews, W.A., Guest, B., 2017. A practical approach for collecting large-n detrital zircon U-Pb data sets by quadrupole LA-ICP-MS. *Geostand. Geoanal. Res.* 41 (2), 161–180.
- Meinhold, G., Morton, A.C., Fanning, C.M., Frei, D., Howard, J.P., Phillips, R.J., et al., 2011. Evidence from detrital zircons for recycling of Mesoproterozoic and Neoproterozoic crust recorded in Paleozoic and Mesozoic sandstones of southern Libya. *Earth Planet Sci. Lett.* 312 (1–2), 164–175.
- Pastore, G., Baird, T., Vermeesch, P., Bristow, C., Resentini, A., Garzanti, E., 2021. Provenance and recycling of Sahara Desert sand. *Earth Sci. Rev.* 216, 103606.
- Paton, C., Woodhead, J.D., Hellstrom, J.C., Hergt, J.M., Greig, A., Maas, R., 2010. Improved laser ablation U-Pb zircon geochronology through robust downhole fractionation correction. *G-cubed* 11.
- Paton, C., Hellstrom, J., Paul, B., Woodhead, J., Hergt, J., 2011. Iolite: freeware for the visualisation and processing of mass spectrometric data. *J. Anal. Atomic Spectrom.* 26 (12), 2508–2518.
- Penaye, J., Kröner, A., Toteu, S.F., Van Schmus, W.R., Doumnang, J.C., 2006. Evolution of the Mayo Kebbi region as revealed by zircon dating: an early (ca. 740 Ma) Pan-African magmatic arc in southwestern Chad. *J. Afr. Earth Sci.* 44 (4–5), 530–542.
- Persits, F.M., Ahlbrandt, T.S., Tuttle, M.L., Charpentier, R.R., Brownfield, M.E., Takahashi, K.L., 1997. *Maps Showing Geology, Oil and Gas Fields and Geological Provinces of Africa* (No. 97-470-A). US Geological Survey.
- Pullen, A., Ibáñez-Mejía, M., Gehrels, G.E., Ibáñez-Mejía, J.C., Pecha, M., 2014. What happens when n= 1000? Creating large-n geochronological datasets with LA-ICP-MS for geologic investigations. *J. Anal. Atomic Spectrom.* 29 (6), 971–980.
- Pullen, A., Ibáñez-Mejía, M., Gehrels, G.E., Giesler, D., Pecha, M., 2018. Optimization of a laser ablation-single collector-inductively coupled plasma-mass spectrometer (thermo element 2) for accurate, precise, and efficient zircon U-Th-Pb geochronology. *G-cubed* 19 (10), 3689–3705.
- Rittner, M., Vermeesch, P., Carter, A., Bird, A., Stevens, T., Garzanti, E., et al., 2016. The provenance of Taklamakan desert sand. *Earth Planet Sci. Lett.* 437, 127–137.
- Saylor, J.E., Sundell, K.E., 2016. Quantifying comparison of large detrital geochronology data sets. *Geosphere* 12 (1), 203–220.
- Saylor, J.E., Jordan, J.C., Sundell, K.E., Wang, X., Wang, S., Deng, T., 2018. Topographic growth of the Jishi Shan and its impact on basin and hydrology evolution, NE Tibetan Plateau. *Basin Res.* 30 (3), 544–563.
- Schuster, M., Roquin, C., Düringer, P., Brunet, M., Caugy, M., Fontugne, M., et al., 2005. Holocene lake Mega-Chad palaeoshorelines from space. *Quat. Sci. Rev.* 24 (16–17), 1821–1827.
- Seignobos, C., Iyébi-Mandjek, O. (Eds.), 2017. *Atlas de la province extrême-nord Cameroun*. IRD Éditions.
- Shellnutt, J.G., Yeh, M.W., Pham, N.H.T., Lee, T.Y., 2019. Cryptic regional magmatism in the southern saharan metacraton at 580 Ma. *Precambrian Res.* 332, 105398.
- Stevens, T., Carter, A., Watson, T.P., Vermeesch, P., Andò, S., Bird, A.F., et al., 2013. Genetic linkage between the yellow river, the mu us Desert and the Chinese loess plateau. *Quat. Sci. Rev.* 78, 355–368.
- Vermeesch, P., 2013. Multi-sample comparison of detrital age distributions. *Chem. Geol.* 341, 140–146.
- Vermeesch, P., 2021. On the treatment of discordant detrital zircon U–Pb data. *Geochronology* 3, 247–257.
- Washington, R., Todd, M.C., Lizcano, G., Tegen, I., Flamant, C., Koren, I., et al., 2006. Links between topography, wind, deflation, lakes and dust: the case of the Bodélé Depression, Chad. *Geophys. Res. Lett.* 33 (9).
- Wiedenbeck, M., Alle, P., Corfu, F., Griffin, W.L., Meier, M., Oberli, F., Vonquadt, A., Roddick, J.C., Speigel, W., 1995. 3 natural zircon standards for U-Th-Pb, Lu-Hf, trace-element and REE analyses. *Geostand. Newsl.* 19 (1), 1–23.